Wavelet-based analysis of enstrophy transfers in two-dimensional turbulence

Patrick Fischer and Charles-Henri Bruneau
IMB Université Bordeaux 1, INRIA Team MC², CNRS UMR 5251, 351, cours de la Libération, 33405 Talence, France

(Received 7 November 2008; accepted 11 May 2009; published online 19 June 2009)

Two-dimensional turbulence admits two different ranges of scales: a direct enstrophy cascade from the injection scale to the small scales and an inverse energy cascade at large scales. It has already been shown in previous papers that vortical structures are responsible for the transfers of energy upscale while filamentary structures are responsible for the forward transfer of the enstrophy. Here we propose an original mathematical tool, the interaction function, for studying the space localization of the enstrophy fluxes. It is defined using an orthogonal two-dimensional wavelet decomposition. © *2009 American Institute of Physics*. [DOI: 10.1063/1.3153910]

I. INTRODUCTION

Two-dimensional turbulence has interested and continues to interest different scientific communities. Its relevance to atmospheric and oceanic flows at large scales has largely motivated its detailed study.[1–3] Its importance for the understanding of turbulence, in general, due to the existence of two cascades, as opposed to the direct cascade of energy in three dimensional turbulence, is another reason to study this phenomenon. While three dimensional turbulence is governed by a direct cascade of energy from the scale of injection to the small scales where the energy is dissipated, two-dimensional turbulence admits two different ranges.[4,5] The first one is governed by an inverse energy cascade from the scale of injection to the large scales. The second one is governed by a cascade of enstrophy from the scale of injection to the small scales. This scenario, proposed by Kraichnan and Batchelor over 40 years ago, finds confirmation in many different numerical simulations and experimental realizations (see, for example, Refs. 6–11). According to the Kraichnan theory, at large scales, the energy spectrum has the form $E(k) \propto k^{-5/3}$ while at small scales it is $E(k) \propto k^{-3}$. However, for the direct cascade at small scales,[12–17] found spectra steeper than k^{-3} in earlier simulations and experiments. We also observed steeper energy spectra in our particular two-dimensional set up[18–20] confirming these earlier results.

Two distinct kinds of structures can be detected in two-dimensional turbulent flows: vortical structures and filamentary structures. The first play an important role for the inverse transfers of energy while the filamentary structures can be associated with the forward transfers of enstrophy. These links between the presence of structures and the transfer of energy or enstrophy have been observed by many authors as Refs. 17 and 19–23.

The inverse energy cascade, whose the merging of same sign vortices is probably one of the mechanisms, transfers energy from the injection scale to the large scales. At scales smaller than the injection scale, an enstrophy cascade, whose origin is certainly the straining of vorticity gradients, transfers enstrophy from large to small scales. The wavelet decompositions used for filtering the turbulent flows have been introduced and extensively studied by Farge and Rabreau since 1988 (Refs. 24 and 25; see also her webpage for an exhaustive list of publications: http://wavelets.ens.fr). However, the usual wavelet-based methods do not allow us to get a precise space localization of the enstrophy fluxes. We know, according to the classical theory and to numerous numerical simulations, that the enstrophy transfers are small-scale physical transfers. We also know that the filamentary structures are responsible for these transfers. However, we do not know yet if these transfers uniformly occur everywhere in the flow and if not, where these transfers precisely take place. Very recent work points out that the mechanism behind these two cascades is the thinning of vortices.[21,22] Stretching of small-scale vorticity gradient by the strain arising from larger-scale vortices is believed to be the mechanism for the enstrophy cascade. Thus the forward enstrophy flux should mainly occur in strain-dominated regions of the flow. Using a Gaussian-based filtering and the Weiss criterion,[26] Ref. 21 showed that the enstrophy flux is either forward or backward with almost equal likelihood in vorticity regions, but tends to be mainly forward in the strain regions. However, this scale Gaussian-based filtering is unable to accurately detect the very spatially localized events responsible for the enstrophy cascade. Quoting,[17] "*Local fluxes are strongly inhomogeneous in physical space: there are relatively small regions of intense (positive and negative) flux in both the energy and enstrophy inertial ranges*," we propose here a complementary mathematical tool for the analysis of the enstrophy flux. We call this mathematical object the interaction function since it describes the interactions responsible for the enstrophy transfers in the flow. It is based on two-dimensional orthogonal wavelet decompositions of the two terms involved in the transport term of the Navier–Stokes equations.

II. THE INTERACTION FUNCTION

The motion of an incompressible viscous fluid in a two-dimensional channel may be described by the vorticity equation obtained by taking the curl of the Navier–Stokes equation:

$$\frac{\partial \omega}{\partial t} + (\boldsymbol{v} \cdot \boldsymbol{\nabla})\omega = \frac{1}{\mathrm{Re}}\nabla^2\omega + f. \quad (1)$$

The velocity field is denoted by $\boldsymbol{v}=(u,v,0)$ and the vorticity by $\omega=\boldsymbol{\nabla}\times\boldsymbol{v}=(0,0,\omega)$ with $\omega=(\partial v/\partial x)-(\partial u/\partial y)$. In Eq. (1), $(\boldsymbol{v}\cdot\boldsymbol{\nabla})\omega$ is the transport term, $(1/\mathrm{Re})\nabla^2\omega$ the dissipation term due to the viscosity and f a potential forcing term. In the computations presented in the sequel, the forcing term is taken equal to zero and the turbulence is naturally created by obstacles in a channel.

The enstrophy flux derives from the nonlinear transport term in the vorticity equation written in Fourier space

$$\Pi_Z(k) = \int_k^{+\infty} T_Z(k')dk', \quad (2)$$

where the enstrophy transfer function $T_Z(k)$ is obtained by angular integration of $N_Z(\omega)=\widehat{\omega^*(\boldsymbol{k})}\cdot\widehat{(\boldsymbol{v}\cdot\boldsymbol{\nabla})\omega(\boldsymbol{k})}$.

We can replace the Fourier transform by a wavelet transform leading to a different representation of the enstrophy transfers in the flow. The method we propose here leads to an original representation, called the enstrophy interaction function. The term $N_Z(\omega)$ is, in fact, a scalar product, in Fourier space, between the vorticity field ω and its transported field $(\boldsymbol{v}\cdot\boldsymbol{\nabla})w$. If the transported field is spectrally close to the initial vorticity field then $N_Z(\omega)$ will be large but if it is very different or even orthogonal then $N_Z(\omega)$ will be insignificant. So, the term $N_Z(\omega)$ measures the correlation, in Fourier space, between the transported and the initial vorticity fields. This correlation is then used to compute the transfer function T_Z and the enstrophy flux Π_Z. By using a Fourier transform, we obtain a description of the enstrophy transfers through the scales, but all the information about the space localization of these transfers is completely lost. However, it is well known, from the classical theory of two-dimensional turbulence and from numerical experiments, that the direct enstrophy cascade takes place from the injection scale to the smallest scales. The enstrophy cascade is thus essentially a small scales phenomenon and may be localized in space. The method we propose in this paper is based on a two-dimensional wavelet transform and leads to a space-scale description of the enstrophy transfers. It consists in replacing the usual Fourier transform in the computation of $N_Z(\omega)$ by a wavelet transform. The interaction function for the enstrophy transfer is obtained through a three step process:

(1) Computation of the two-dimensional orthogonal wavelet transforms of $\omega(\boldsymbol{k})$ and $(\boldsymbol{v}\cdot\boldsymbol{\nabla})\omega(\boldsymbol{k})$. This step leads to the space-scale representations of these two terms. The results of these transforms are denoted by $\mathrm{WT}(\omega)$ and $\mathrm{WT}((\boldsymbol{v}\cdot\boldsymbol{\nabla})\omega)$ in the sequel.
(2) Computation of the scalar product of $\mathrm{WT}(\omega)$ and $\mathrm{WT}((\boldsymbol{v}\cdot\boldsymbol{\nabla})\omega)$. The result of this product is a wavelet-based representation of the interactions responsible for the enstrophy transfers. The coefficients obtained here will be strong if the strong coefficients of $\mathrm{WT}(\omega)$ and $\mathrm{WT}((\boldsymbol{v}\cdot\boldsymbol{\nabla})\omega)$ are localized at the same place and the same scale. In the usual enstrophy flux computation in Fourier space, the space information is completely lost and only scale localizations are considered.
(3) Reconstruction in the physical space, using an inverse wavelet transform, of the result obtained at the previous step. This last step restitutes in physical space the interactions between $\mathrm{WT}(\omega)$ and $\mathrm{WT}((\boldsymbol{v}\cdot\boldsymbol{\nabla})\omega)$ occurring at various scales. The result of this last computational step is by definition the interaction function and is denoted by IF_Z.

This three steps algorithm can be summarized by the formula

$$\mathrm{IF}_Z = \mathrm{WT}^{-1}[\mathrm{WT}(\omega)\mathrm{WT}((\boldsymbol{v}\cdot\boldsymbol{\nabla})\omega)], \quad (3)$$

where WT denotes the two-dimensional wavelet transform and WT^{-1} its inverse transform. The interaction function is used by itself, but is not used to compute the enstrophy flux which does not give any spatial information. It can be conveniently represented onto a contour plot of the vorticity field. No thresholding is applied on the wavelet coefficients, but the color representation enhances the regions corresponding to strong enstrophy interactions. So the wavelet transform gives a space-scale representation of the object under study. When performing the scalar product, we compare, in fact, the wavelet decompositions of the two terms involved in the product. If the two terms have the same behavior at the same place and the same scale then the result of the scalar product will present large coefficients at the corresponding scale and place. Then by applying an inverse wavelet transform we can get a space representation of the interactions involved in the enstrophy transfers. The same process can be used for the energy transfers using the corresponding data.

III. NUMERICAL TESTS ON TWO TEXTBOOK CASES

A first textbook case of the interaction function is given in Fig. 1. This figure corresponds to the simulation of the evolution of two vortices of different signs in a 2π periodic square domain. After a while a third but less energetic vortex is created. The interaction function mainly focus on the two original vortices where the strong interactions take place. A second textbook case is presented in Figs. 2 and 3. In this experiment, 14 vortices of different signs have been randomly dispatched in a 2π periodic square domain. During the decaying process, some vortices merged and we obtained the vorticity field shown in Fig. 2. As can be easily noticed, the interaction function points to one particular event. Computing the enstrophy fluxes corresponding to the whole flow and to a small area delimited by the interaction function allows us to show that the interaction function effectively points to the main event in the flow (Fig. 3).

The relevance and the interest of the interaction function cannot be fully assessed on mere examples like those presented here since they correspond to decaying homogeneous isotropic turbulent flows and thus the notion of enstrophy cascade is limited. The power of this new mathematical function is presented in the next part where fully developed turbulence simulations are carefully analyzed.

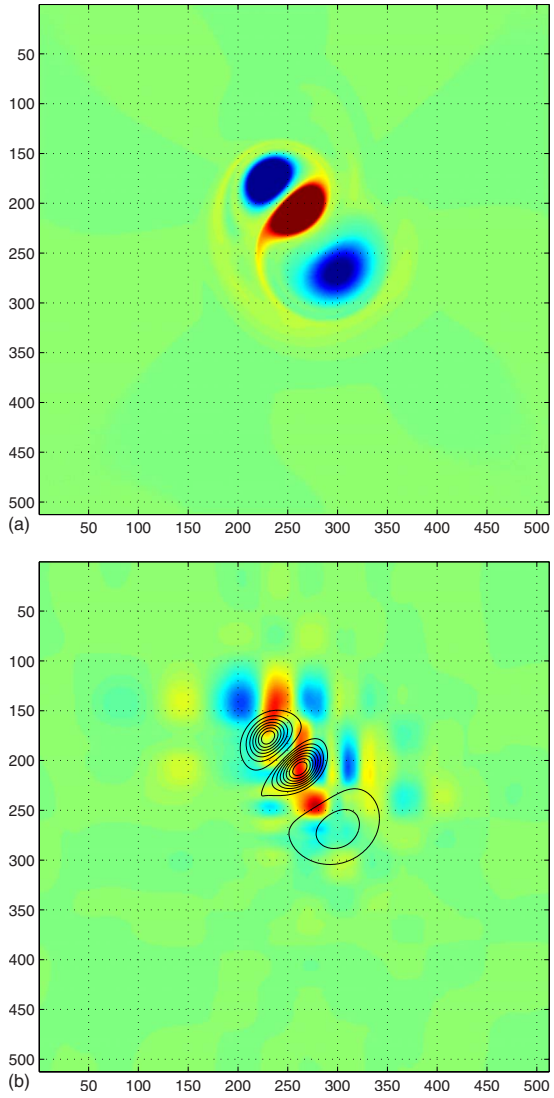

FIG. 1. (Color online) Two vortices interacting and giving birth to a third one. (a) Vorticity field. (b) Interaction function with contour lines of vorticity.

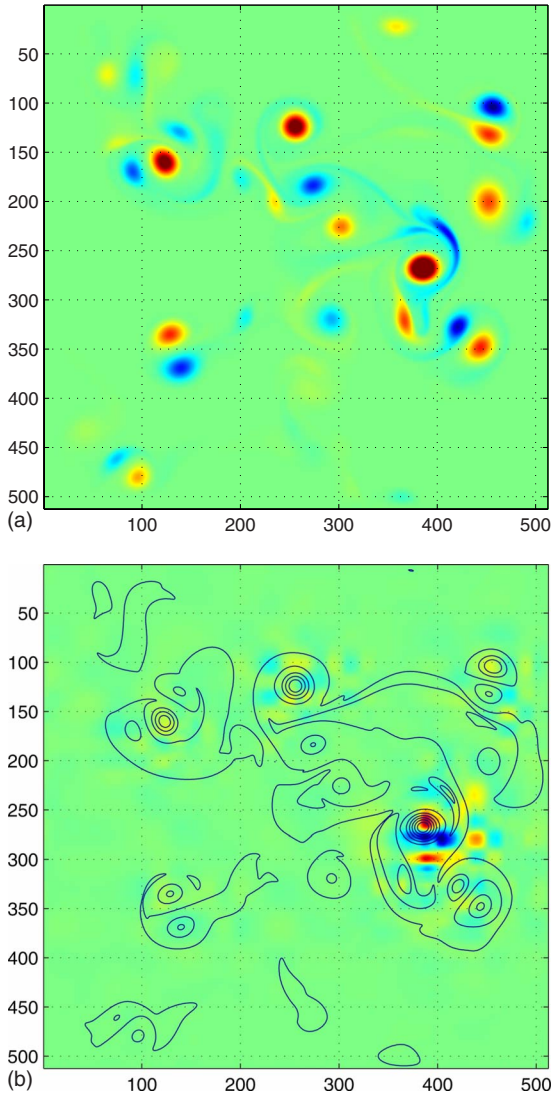

FIG. 2. (Color online) Fourteen vortices of different signs interacting in a 2π periodic domain. (a) Whole vorticity field. (b) Interaction function with contour lines of vorticity.

IV. EXPERIMENTAL SETUP

The numerical experiments presented in this paper have been originally motivated by experiments carried out with soap films where grid turbulence was studied in details.[13,27] They consist in the numerical simulation of a two-dimensional channel flow perturbed by an horizontal array of cylinders. Two vertical arrays of additional cylinders have been added in order to increase the number of vortices, and thus to enhance the turbulent behavior of the flow.[18] The numerical results obtained through such direct numerical simulation are the same than those discussed in Ref. 18. They can be compared to those obtained by soap film experiments where the flow is perturbed by analogous arrays of small cylinders.[18]

This unusual set up is more related to realistic cases than the classical two-dimensional periodic domain approach. It corresponds to a river flowing under a bridge with the cylinders playing the role of the bridge pillars. Furthermore, the production of vorticity by real physical boundaries cannot be studied with classical periodic domain conditions and requires particular set up as we study here. Indeed, the numerical setup and the interaction function method presented here are particularly well adapted for studying boundary vorticity creation.

The length of the rectangular channel Ω is four times its width L and the Reynolds number based on the cylinders diameter is $\mathrm{Re}=5000$. In this experiment, the cylinders create and maintain the turbulent behavior of the flow. Thus the injection scale k_{inj} is given by the diameter of cylinders $L/8$ and consequently the injection scale is around $k_{\mathrm{inj}}=8$. We use here a large injection scale as we focus on the enstrophy cascade range (Fig. 4).

The penalization method is used to solve the flow around the obstacles. Consequently the Brinkman–Navier–Stokes equations are solved in the whole channel Ω including the solid obstacles Ω_s and the fluid domain Ω_f. This problem has been theoretically studied in Ref. 28.

The equations are discretized in time by a second-order Gear scheme with an implicit treatment of the linear terms

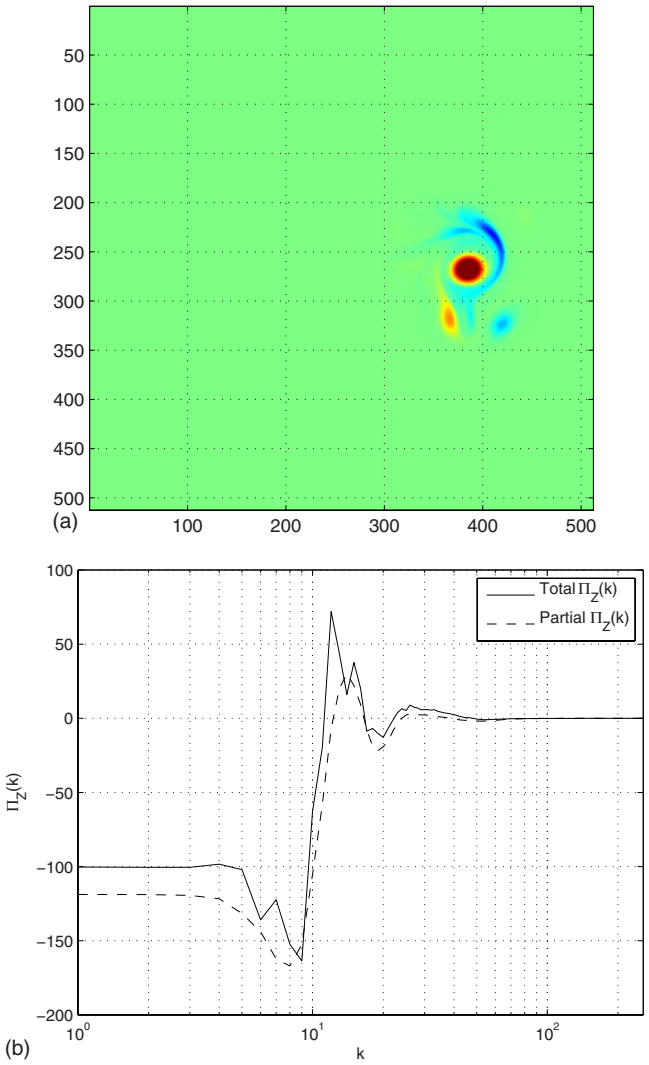

FIG. 3. (Color online) Fourteen vortices of different signs interacting in a 2π periodic domain. (a) Partial vorticity field. (b) Enstrophy fluxes for the whole flow and for the selected area.

and an explicit treatment of the convection term. The spatial approximation is performed on uniform staggered grids using second-order centered finite differences for the linear terms and a third-order upwind scheme for the convection term.[29] The location of the unknowns enforce the divergence-free equation which is discretized on the pressure points and the choice of uniform grids is necessary to maintain the accuracy of the finite differences schemes. The whole problem is solved by a multigrid method with a cell by cell Gauss–Seidel iterative procedure as smoother. A sequence of grids from 4×16 cells up to 1024×4096 cells is used on the domain $\Omega=(0,1)\times(0,4)$ to get accurate results.

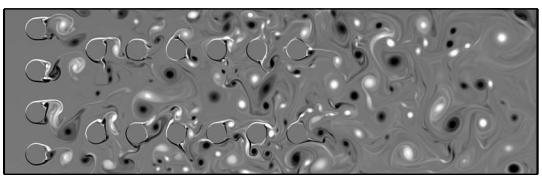

FIG. 4. Snapshot of the vorticity field.

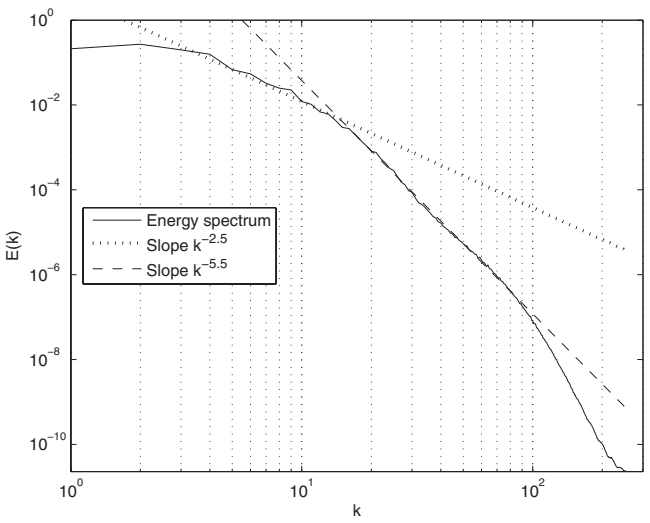

FIG. 5. Energy spectrum.

With respect to the Reynolds number, the finest grid is fine enough to properly capture the whole dynamics.

Several wavelet bases have been used to test the validity of the interaction function. They all point to the same localizations for the enstrophy transfers, even if the colored patterns were not exactly the same. The method does not depend on the choice of the wavelet basis used in the computations. The results obtained with Daubechies wavelets with ten vanishing moments are presented in here. The wavelet decompositions have been performed over all the scales (ten for this grid).

V. NUMERICAL RESULTS

The computation of the enstrophy flux has been performed for different configurations (several Reynolds numbers, several diameters for the obstacles) and many snapshots of the flow for each configuration. We present here the results obtained for a series of 100 images. A snapshot of the vorticity field from the upstream cylinders to the end of the channel is given in Fig. 4. To compute the energy spectrum and the enstrophy flux, we select a square of size $L=1$ located at the end of the channel as domain of analysis. The cutting process to select this domain creates many discontinuities in the velocity and vorticity fields at the boundaries, and thus introduces high frequency Fourier coefficients. This phenomenon is well known from people using the classical fast Fourier transform (FFT) algorithm and has been described in Refs. 20 and 30. We avoid this problem by using a windowed Fourier transform that removes the spurious coefficients created by the discontinuities. We use, for the results presented in this paper, a Tukey window with a parameter equal to 0.1. A larger value for this parameter would cancel a too large amount of the energy and the enstrophy, and a smaller one would not sufficiently smooth the discontinuities. The averaged energy spectrum for the 100 first snapshots is given in Fig. 5. We can observe two slopes on both sides of the injection scale, the first slope being around $k^{-2.5}$ and the second one around $k^{-5.5}$ and so far from the classical theory that predicts a decrease in k^{-3}. The first slope is not

really clear but the second one is evident. Many papers in literature discussed the influence of solid boundaries on the evolution of two-dimensional turbulence in a finite domain.[31–35] According to these studies, the classical theory proposed by Refs. 4 and 5 does not take into account the effects of these particular boundary conditions. Indeed according to Ref. 34, no-slip walls are sources of vorticity filaments which may affect the behavior of two-dimensional turbulence. Furthermore, they could show that their influence are not restricted to regions close to the boundary but also extend over the full domain. In our experiments, due to the presence of many cylinders, the flow is dominated by vortices created by the cylinders and vorticity filaments in between.

The enstrophy flux corresponding to this spectrum is given in Fig. 6. The enstrophy flux is positive above the injection scale, and negative below. The zero crossing corresponds approximately to the injection scale. Our simulations do not produce a large plateau but an explanation for this is the limitation of range of scales probed and the presence of the boundaries. In our mathematical model, we did not use any artificial dissipation terms which would improve the creation of the cascades.

The flux presented in Fig. 6 is, in fact, a mean obtained by averaging 100 snapshot fluxes, but does not correspond to the flux of any snapshot. In order to assess the local interactions in the flow, we have to study the flux of few snapshots separately. We can represent the fluxes of the 100 snapshots in one color representation. The color map goes from blue for negative values to red for positive values. The wavenumber range extends from $k=1$ to $k=100$ since no flux could be obtained beyond. This representation is given in Fig. 7. We can observe that some snapshots present a strong direct enstrophy flux, and others a strong inverse flux leading to the average given in Fig. 6. We can find a very few snapshots with the inverse and direct fluxes in the same time. This proves that the direct enstrophy cascade is not a permanent phenomenon, but rather a transient phenomenon that alternates with an inverse enstrophy cascade. It can be noticed that these inverse enstrophy flux periods coincide with strong inverse energy flux periods. It is not surprising that strong energy transfers carry also some enstrophy with them. As can be also observed, the inverse energy cascade is only localized between $k=1$ and the injection scale $k=8$ in accordance with the classical theory.

A. Interaction function for the whole field

In order to study the interactions occurring into the enstrophy cascade, the interaction function is now computed for few snapshots with strong direct enstrophy fluxes. Snapshots 85 and 92 have been chosen for that purpose. The vorticity field corresponding to snapshot 85 is given in Fig. 8(a). Various structures can be observed in this vorticity field. According to previous studies,[19,23] we already know that the vorticity filaments are responsible for the inverse enstrophy cascade, but we do not have yet any information

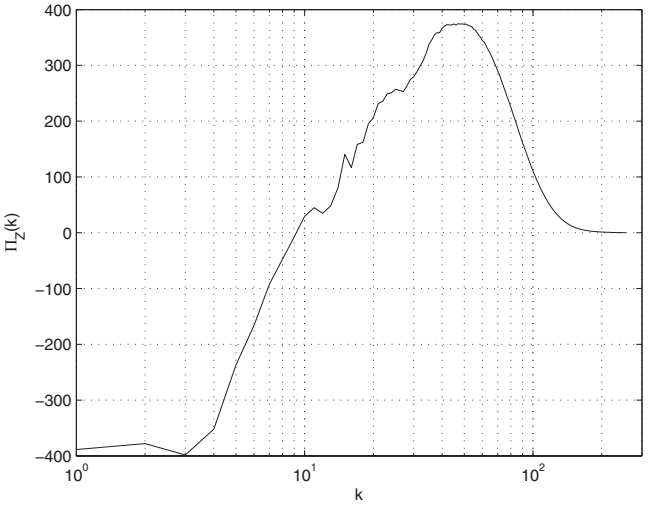

FIG. 6. Enstrophy flux.

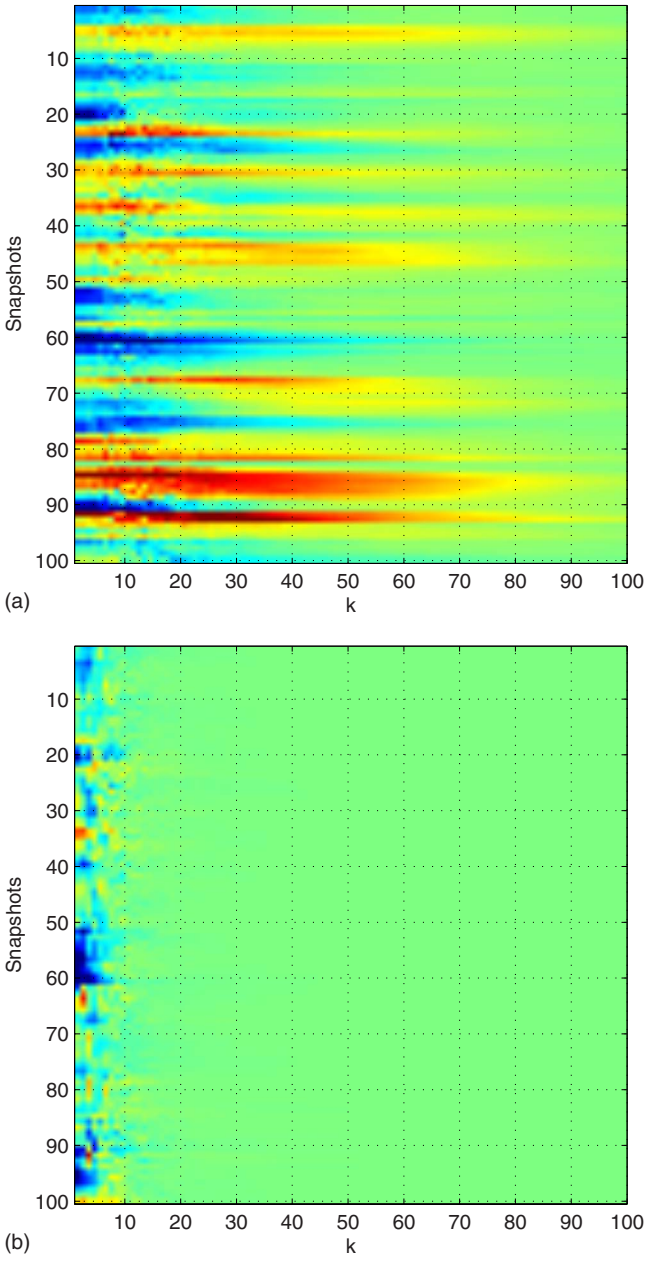

FIG. 7. (Color online) Fluxes for 100 snapshots. (a) Enstrophy flux. (b) Energy flux.

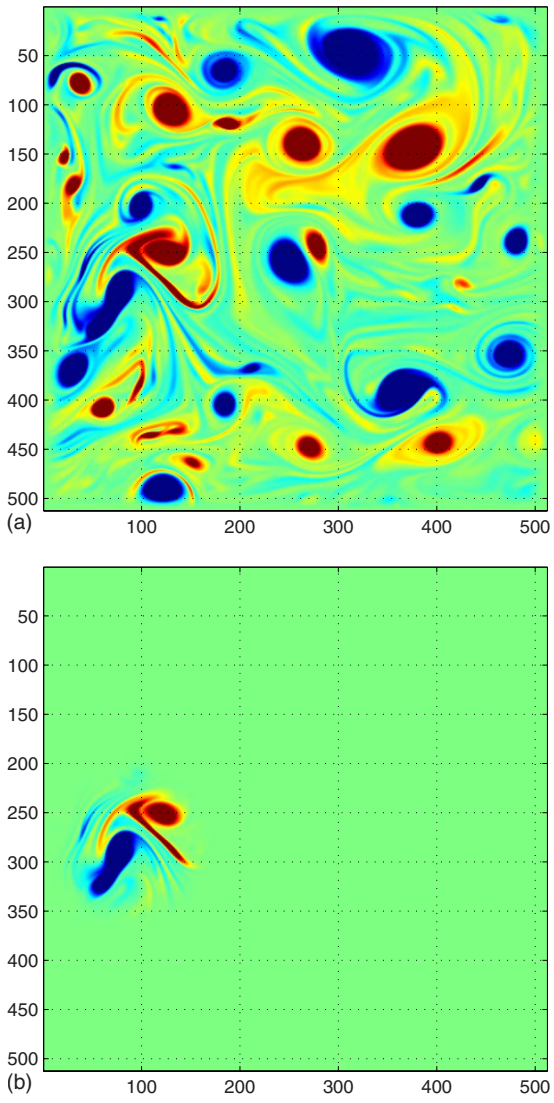

FIG. 8. (Color online) Snapshot 85. (a) Vorticity field. (b) Partial vorticity field.

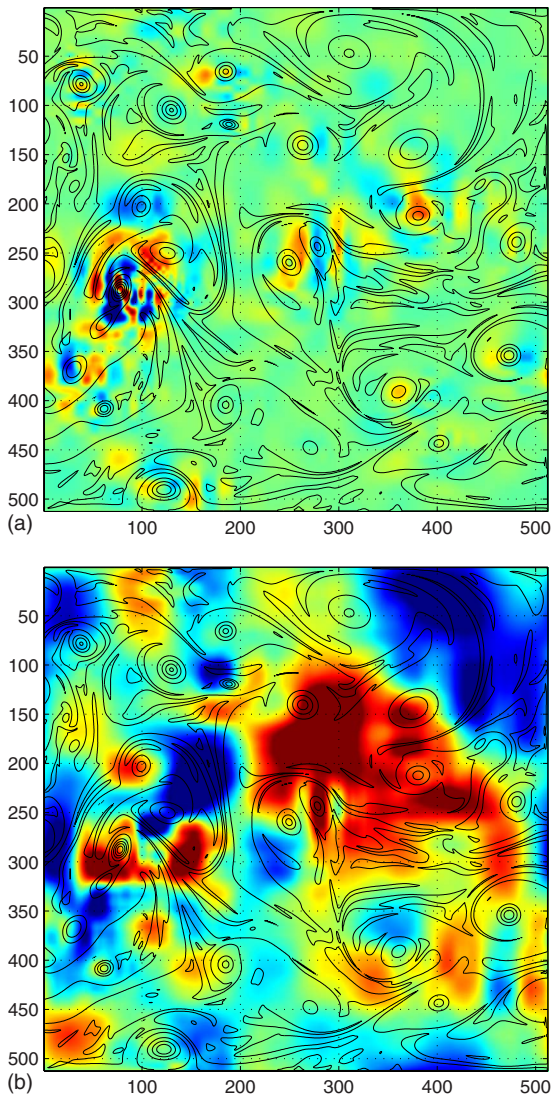

FIG. 9. (Color online) Snapshot 85 (vorticity field in contour lines). (a) Enstrophy interaction function. (b) Energy interaction function.

about the space localization of the interactions leading to this cascade. The enstrophy interaction function, represented in Fig. 9(a), allows us to get this kind of information. The contrast and the color map have been chosen such that only the most important coefficients are noticeable. Tuning the contrast would make regions appear more colored corresponding to weak enstrophy fluxes. In this snapshot, a region with strong values around (90,285) can be detected. This zone corresponds to interactions between two vortices of opposite signs and where most of the enstrophy cascade occurs. This can be verified by computing the total enstrophy flux and the partial one corresponding to this region. Different strategies can be developed to select this area. We first chose all the points where the enstrophy interaction function is greater than a given threshold (here, the average value between the absolute value maximum and the absolute value mean of the snapshot), and then chose a Gaussian mask that included all these points. The total and partial enstrophy fluxes are given in Fig. 10 and the selected area in the vorticity field in Fig. 8(b). As expected, the partial enstrophy flux almost fits the

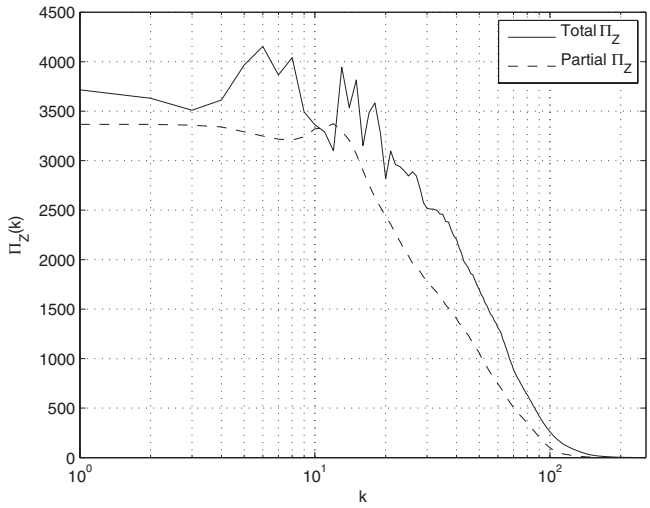

FIG. 10. Enstrophy fluxes (snapshot 85).

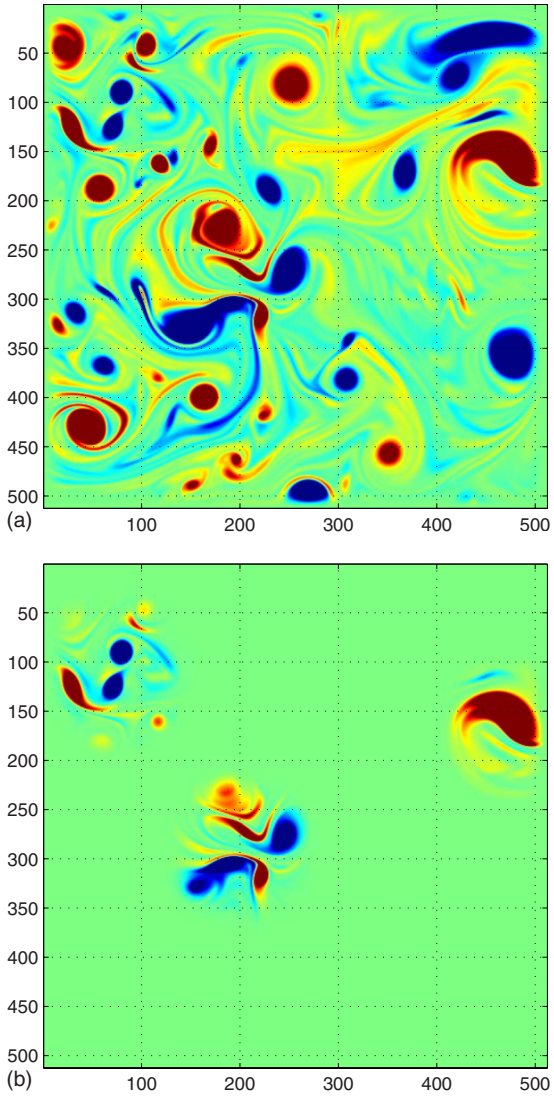

FIG. 11. (Color online) Snapshot 92. (a) Vorticity field. (b) Partial vorticity field.

total enstrophy flux proving that the main interactions creating the enstrophy cascade effectively take place in this region. About 80% of the total enstrophy flux takes place in less than 15% of the flow surface. The energy interaction function, computed in the same way as the enstrophy interaction function, is given in Fig. 9(b). The inverse energy cascade taking place at larger scales, one can observe large regions of interactions for the energy. Consequently, a local analysis of the energy fluxes is not relevant.

A single area of strong interactions has been detected by the interaction function in this snapshot. However, it may happen in some cases that the enstrophy flux is due to interactions localized in multiple small areas. In this case, the interaction function is still able to precisely locate them as can be verified with the following example. The same kind of analysis is now repeated for snapshot 92 [vorticity field given in Fig. 11(a)]. The corresponding interaction functions are given in Fig. 12.

We can observe that the interactions occur in three different places. A smaller area around (425,75) can be visually detected in Fig. 12(a) but failed the automatic quantitative selection process. This area could be included in the selected zones group by slightly modifying our threshold. The partial enstrophy flux computed with this fourth zone would be even closer to the total enstrophy flux. The partial and the total vorticity fields are given in Fig. 11. These three areas correspond to places where interactions between different objects occur. We can then compare the total enstrophy flux to the partial one obtained with the three selected regions. The results are given in Fig. 13. For this snapshot too, the enstrophy flux computed in the selected areas almost fits the total enstrophy flux proving that the main interactions creating the enstrophy cascade effectively take place in these three regions. The energy interaction function shows also larger activity area but smaller than those obtained for snapshot 85.

B. Interaction function for the filtered fields

Using the same kind of filtering as in Refs. 19, 20, and 23, the velocity fields can be cut into two subfields: one subfield with the solid rotation part of the vortices (denoted by the subscript s) and the remaining mainly composed of vorticity filaments that roll up in spiral inside the vortices (denoted by the subscript f). The velocity decomposition $\boldsymbol{v}=\boldsymbol{v}_s+\boldsymbol{v}_f$ obtained with the wavelet packets based filtering is orthogonal and leads to the energy spectrum decomposition

$$E(k) = E_s(k) + E_f(k), \tag{4}$$

where E_s is the energy of the solid rotation vortices and E_f is the energy of the vorticity filaments. Due to this orthogonal decomposition, the enstrophy transfer function can be written as

$$\begin{aligned} T_Z(\boldsymbol{k}) &= \widehat{\omega^*(\boldsymbol{k})} \cdot \widehat{(\boldsymbol{v}\cdot\nabla)\omega(\boldsymbol{k})} \\ &= \widehat{\omega_s^*(\boldsymbol{k})} \cdot \widehat{(\boldsymbol{v}\cdot\nabla)\omega_s(\boldsymbol{k})} + \widehat{\omega_s^*(\boldsymbol{k})} \cdot \widehat{(\boldsymbol{v}\cdot\nabla)\omega_f(\boldsymbol{k})} \\ &\quad + \widehat{\omega_f^*(\boldsymbol{k})} \cdot \widehat{(\boldsymbol{v}\cdot\nabla)\omega_s(\boldsymbol{k})} + \widehat{\omega_f^*(\boldsymbol{k})} \cdot \widehat{(\boldsymbol{v}\cdot\nabla)\omega_f(\boldsymbol{k})}. \end{aligned} \tag{5}$$

The same decomposition can be also written for the energy transfer function.

The global enstrophy transfer is thus split into four parts corresponding to the multiscale transfers from one subfield to itself or to the other one. For instance, $\widehat{\omega_s^*}(\boldsymbol{k})\cdot\widehat{(\boldsymbol{v}\cdot\nabla)\omega_f}(\boldsymbol{k})$ is the enstrophy transfer from the vorticity filaments subfield to the solid rotation subfield. The fluxes corresponding to each term in the expression of the total enstrophy transfer function are denoted as, for example, $\Pi_Z^{f\to s}$ which is the flux corresponding to the transfer term previously described. We already know from previous studies[19,20,23] that the filamentary structures are responsible for the enstrophy fluxes. Indeed it has been shown that $\Pi_Z^{f\to f}$ is the main term in Π_Z whereas $\Pi_E^{s\to s}$ is the main term in Π_E.

Moreover, one can specify how these interactions take place or more exactly what are the media allowing those transfers. Indeed, thanks to the decomposition of the transport operator itself, it has been shown in Ref. 23 that the

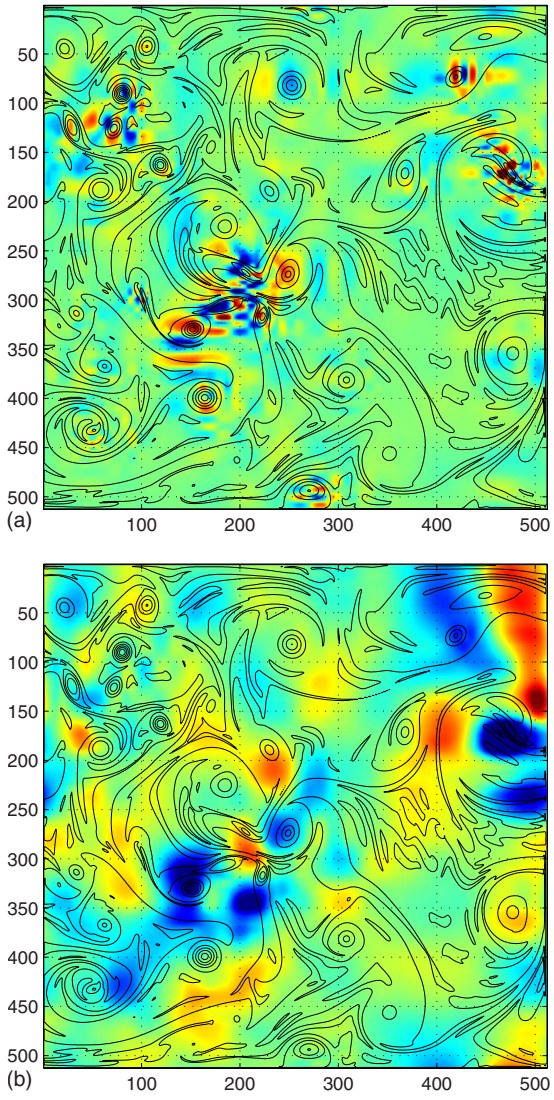

FIG. 12. (Color online) Snapshot 92 (vorticity field in contour lines). (a) Enstrophy interaction function. (b) Energy interaction function.

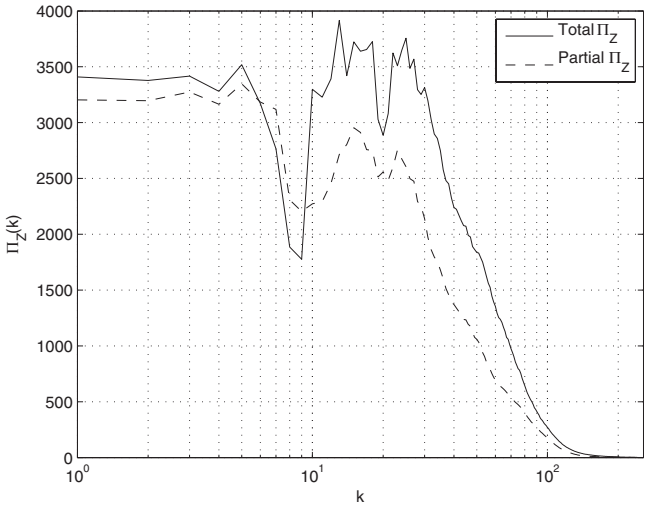

FIG. 13. Enstrophy fluxes (snapshot 92).

solid rotations of the vortices are the means of transport of the energy and enstrophy transfers. Thus the transport operator can be decomposed into two parts:

$$(\boldsymbol{v}\cdot\nabla)=(\boldsymbol{v}_s\cdot\nabla)+(\boldsymbol{v}_f\cdot\nabla). \tag{6}$$

By performing this decomposition one can separate the enstrophy transport operated by the solid rotations from the transport operated by the filaments. Finally each term of Eq. (5) can be also split into two parts leading to the following complete decomposition:

$$\begin{aligned} T_Z(\boldsymbol{k}) = {} & \widehat{\omega_s^*(\boldsymbol{k})}\cdot\widehat{(\boldsymbol{v}_s\cdot\nabla)\omega_s(\boldsymbol{k})}+\widehat{\omega_s^*(\boldsymbol{k})}\cdot\widehat{(\boldsymbol{v}_f\cdot\nabla)\omega_s(\boldsymbol{k})} \\ & +\widehat{\omega_s^*(\boldsymbol{k})}\cdot\widehat{(\boldsymbol{v}_s\cdot\nabla)\omega_f(\boldsymbol{k})}+\widehat{\omega_s^*(\boldsymbol{k})}\cdot\widehat{(\boldsymbol{v}_f\cdot\nabla)\omega_f(\boldsymbol{k})} \\ & +\widehat{\omega_f^*(\boldsymbol{k})}\cdot\widehat{(\boldsymbol{v}_s\cdot\nabla)\omega_s(\boldsymbol{k})}+\widehat{\omega_f^*(\boldsymbol{k})}\cdot\widehat{(\boldsymbol{v}_f\cdot\nabla)\omega_s(\boldsymbol{k})} \\ & +\widehat{\omega_f^*(\boldsymbol{k})}\cdot\widehat{(\boldsymbol{v}_s\cdot\nabla)\omega_f(\boldsymbol{k})}+\widehat{\omega_f^*(\boldsymbol{k})}\cdot\widehat{(\boldsymbol{v}_f\cdot\nabla)\omega_f(\boldsymbol{k})}. \end{aligned} \tag{7}$$

The second term in the right hand side of Eq. (7) describes the enstrophy transfer from the solid rotations to themselves by the filamentary structures. The main term responsible for the enstrophy flux, as shown in Ref. 23, can thus be written as

$$\Pi_Z^{f\to f}=\Pi_Z^{f\to s\to f}+\Pi_Z^{f\to f\to f}, \tag{8}$$

where $\Pi_Z^{f\to s\to f}$ denotes enstrophy transported from filaments to filaments by vortical structures, and $\Pi_Z^{f\to f\to f}$ is the same but by filamentary structures. The interaction functions corresponding to the three terms in Eq. (8) are given in Fig. 14, but those corresponding to the other subfields are not given here because they do not present any strong coefficients. One can remark in Fig. 14 that the strong coefficients are localized at the same place as in Fig. 9. These figures are coherent with the results obtained in Ref. 23: the filamentary structures are responsible for the enstrophy cascade, and the solid rotations (and not the vorticity filaments since there is no strong coefficients for $\Pi_Z^{f\to f\to f}$) transport the enstrophy from the filaments to the filaments. The interaction function provides a new insight in the enstrophy cascade since it shows that the enstrophy transfers are not uniformly spread in the whole flow but are localized in particular regions. In all the experiments we performed, enstrophy transfers occur where different sign vortices interact with each other stretching in new filamentary structures.

C. Attempt of physical interpretations

Many numerical simulations corresponding to different geometries (the same channel but with different numbers of obstacles of various sizes) have been realized and studied. We noticed that some snapshots could present strong direct enstrophy fluxes whereas others present strong inverse enstrophy fluxes. The observations of the corresponding vorticity fields could not give any explanation about this two quite different behaviors. However, the wavelet packets filtering leading to the two subfields associated to the interaction

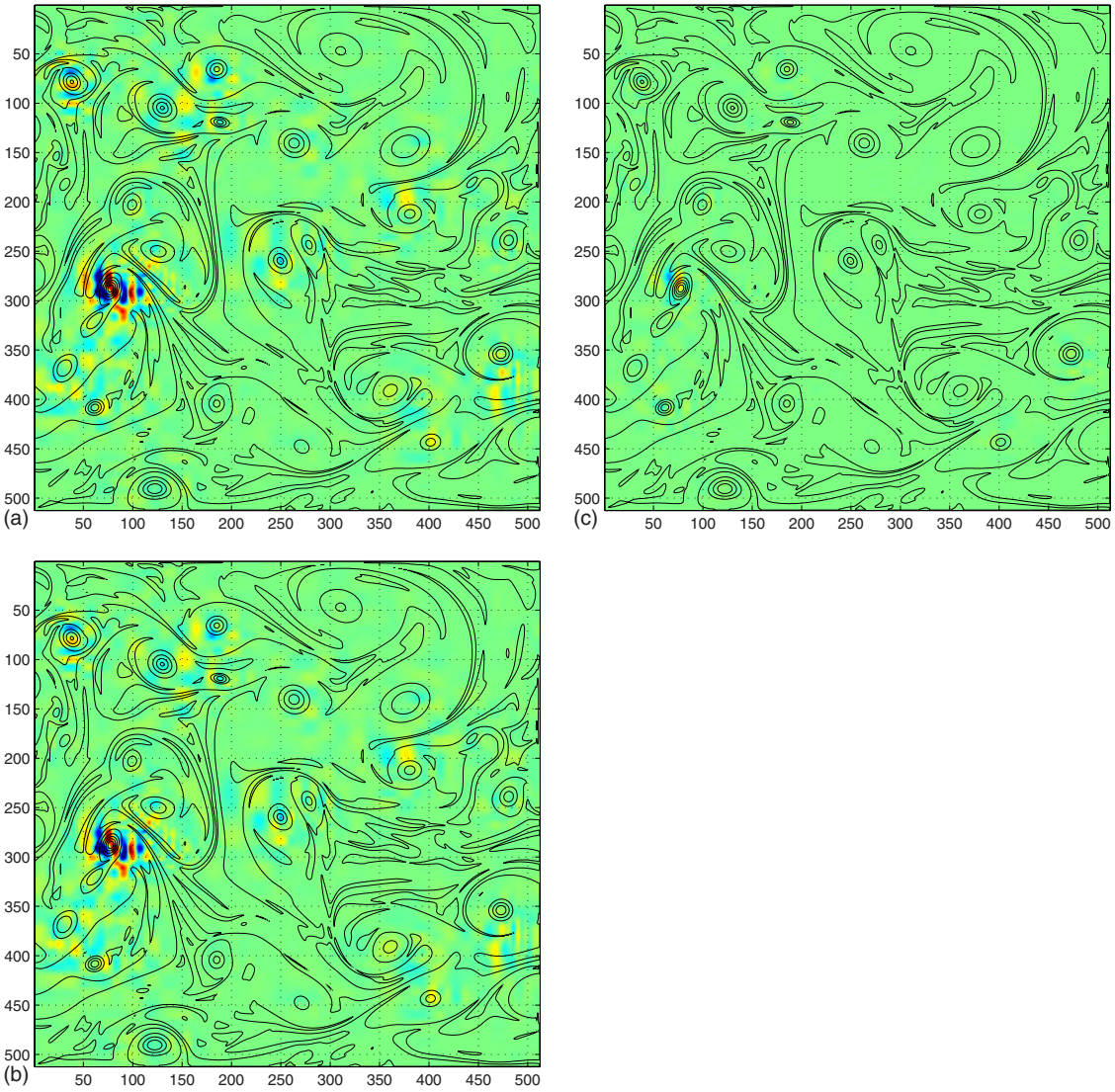

FIG. 14. (Color online) Interaction functions for the filtered fields (snapshot 85). (a) $\Pi_Z^{f\to f}$, (b) $\Pi_Z^{f\to s\to f}$, and (c) $\Pi_Z^{f\to f\to f}$.

function analysis can give some information about the physical process. First, we isolated two of this kind of events from several hundreds available snapshots. They correspond to experiments on a fine grid with ten small cylinders across the channel and nine small cylinders on each side ($k_{\mathrm{inj}} \approx 20$). The corresponding enstrophy interaction functions are given in Fig. 15. As can be seen on these figures, there is one particular zone in each snapshot where the interaction function detects some strong activities. These zones are located around (170, 180) for snapshot 147 and (200, 100) for snapshot 195. The vorticity fields corresponding to these selected zones are given in Fig. 16. The selected zones correspond to places where vortices of different signs interact with each other. We cannot notice any difference between the two snapshots in Fig. 16 that could explain why they do have completely different behaviors from an enstrophy flux point of view. Indeed, if we study their respective enstrophy fluxes (given in Fig. 17) we can notice that snapshot 147 presents a strong inverse enstrophy cascade whereas snapshot 195 has a strong direct cascade. In both cases, the selected zones represent less than 15% of the total surface but more than 80% of the enstrophy fluxes.

However, the interaction function for the whole flow does not give any explanation for the difference of enstrophy behaviors between the two snapshots. However we can find a beginning of explanation when studying the interaction functions of the filtered fields obtained through the wavelet packets filtering process. We compute for each snapshot the interaction functions of the eight terms in Eq. (8). For snapshot 147, we found that the term $\Pi_Z^{s\to s\to s}$ is the dominant term whereas for snapshot 195 the term $\Pi_Z^{f\to s\to f}$ is the main factor in decomposition (8). So in snapshot 195, the enstrophy is transferred from filaments to filaments transported by vortices, leading to the direct enstrophy cascade classical mechanism, whereas in snapshot 147 the enstrophy is transported by vortices from vortices to themselves. A detailed study of the snapshots shows that the mechanism for the direct enstrophy cascade is a strong stretching created by the interactions

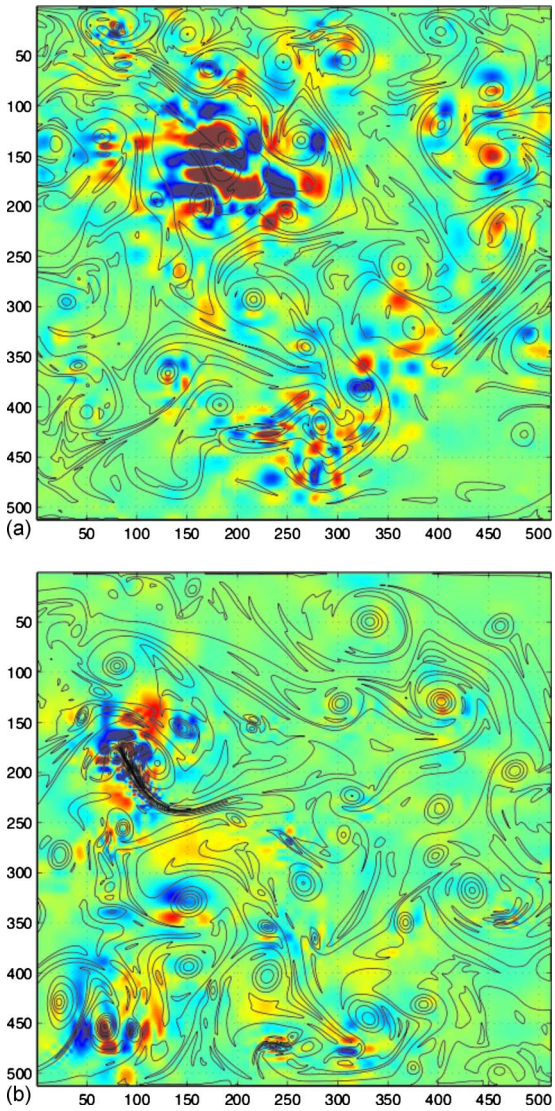

FIG. 15. (Color online) Enstrophy interaction function. (a) Snapshot 147. (b) Snapshot 195.

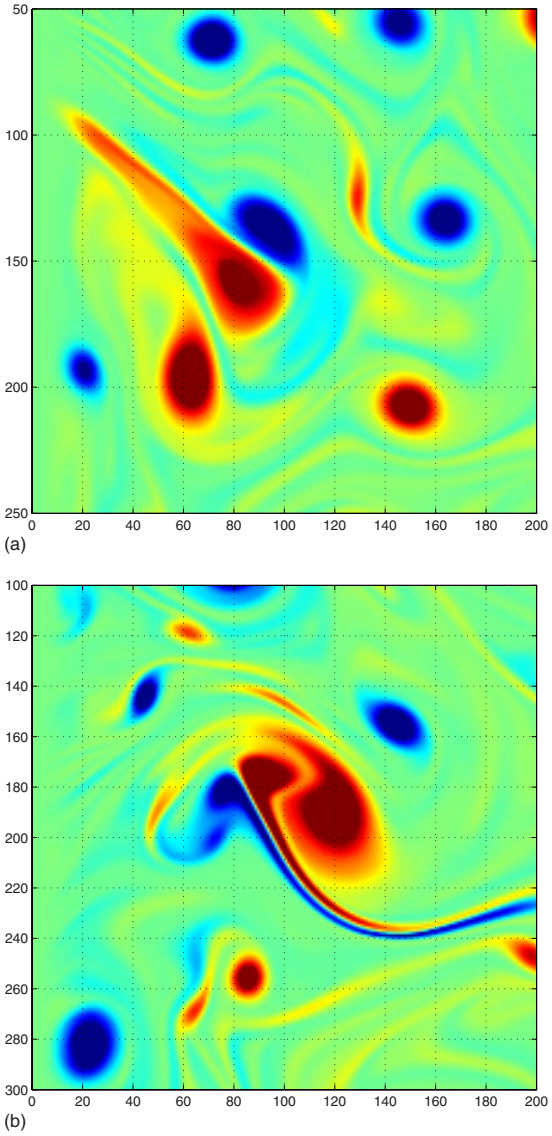

FIG. 16. (Color online) Selected zones of the vorticity fields detected by the interaction function. (a) Snapshot 147. (b) Snapshot 195.

between two vortices of different signs. This stretching creates a long filamentary structure where the transfers are located as it is observed with the corresponding interaction function. We do not see this kind of long filamentary structure in snapshot 195, but we can see the interactions between an elongated vortex and another vortex of the same sign. In this case, we can notice that, according to the interaction function, the main interaction takes place between the two like sign vortices.

VI. CONCLUSION

We propose in this paper an original wavelet-based mathematical tool for studying two-dimensional turbulent flows. This object, called the interaction function, reveals the local enstrophy fluxes in the flow. It is based on the scalar product in a wavelet approximation space of the two terms involved in the computation of the regular enstrophy flux. This study confirms that the enstrophy flux is not a homogeneous phenomenon spread over the whole flow but a local phenomenon corresponding to local interactions. We observed that in most of the cases more than 80% of the enstrophy flux take place in less than 15% of the flow surface. An important application of the interaction function is obtained in association to our regular wavelet packet filtering. Indeed, using these two complementary tools we can observe that inverse enstrophy fluxes are due to interactions between vortices only whereas direct enstrophy fluxes are related to vorticity filaments interactions with vortices. This is mainly a confirmation of what has been thought for a while: the inverse energy cascade is for a large part due to the merging of vortices and the direct enstrophy cascade is for a large part due to the stretching of vortices that produces very long vorticity filaments when they are laminated. In addition, the balance between these two kinds of events governs the level of enstrophy for large scales. When there are more merging events the mean of the enstrophy flux can be negative for scales larger than the injection scale. In the opposite, this mean can be positive when stretching effects dominate in the flow. An important application of our method is related to the

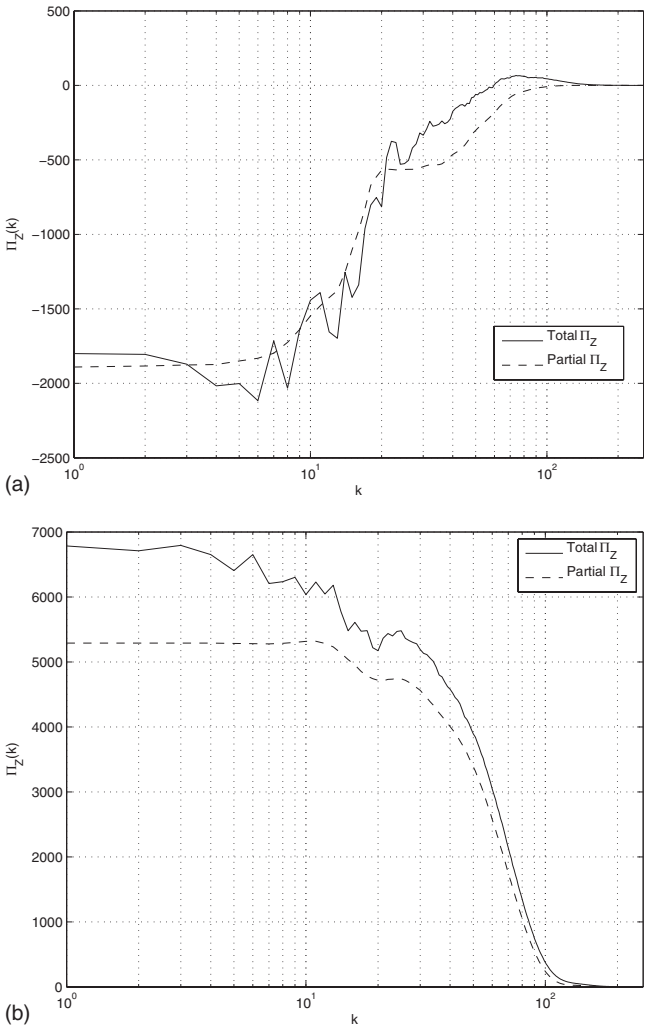

FIG. 17. Enstrophy fluxes for the whole flows and for the selected areas. (a) Snapshot 147. (b) Snapshot 195.

study of the walls influence in a turbulent flow. The interaction function can bring relevant information about the vorticity creation by the boundary layers. This is a challenging and open problem that cannot rely on classical tools and that requires efficient and accurate space-scale techniques. Another application is to follow along the time the vortical structures pointed out by the interaction function to determine the role of the physical events (merging, stretching, etc.).

ACKNOWLEDGMENTS

The authors thank the referees for their valuable and relevant comments about the manuscript.

[1] P. Morel and M. Larcheveque, "Relative dispersion of constant-level balloons in 200mb general circulation," J. Atmos. Sci. **31**, 2189 (1974).
[2] E. Lindborg, "Can the atmospheric kinetic energy spectrum be explained by two-dimensional turbulence?" J. Fluid Mech. **388**, 259 (1999).
[3] K. K. Tung and W. Orlando, "The k-3 and k-5/3 energy spectrum of atmospheric turbulence: Quasigeostrophic two level model simulation," J. Atmos. Sci. **60**, 824 (2003).
[4] R. H. Kraichnan, "Inertial ranges in two-dimensional turbulence," Phys. Fluids **10**, 1417 (1967).
[5] G. K. Batchelor, "Computation of the energy spectrum in homogeneous two-dimensional turbulence," Phys. Fluids **12**, II-233 (1969).
[6] J. Paret and P. Tabeling, "Experimental observation of the two-dimensional inverse energy cascade," Phys. Rev. Lett. **79**, 4162 (1997).
[7] E. Siggia and H. Aref, "Point-vortex simulation of the inverse energy cascade in two-dimensional turbulence," Phys. Fluids **24**, 171 (1981).
[8] U. Frisch and P. L. Sulem, "Numerical simulation of the inverse cascade in two-dimensional turbulence," Phys. Fluids **27**, 1921 (1984).
[9] L. Smith and V. Yakhot, "Bose condensation and small-scale structure generation in a random force driven two-dimensional turbulence," Phys. Rev. Lett. **71**, 352 (1993).
[10] V. Borue, "Spectral exponents of enstrophy cascade in stationary two-dimensional homogeneous turbulence," Phys. Rev. Lett. **71**, 3967 (1993).
[11] V. Borue, "Inverse energy cascade in stationary two-dimensional homogeneous turbulence," Phys. Rev. Lett. **72**, 1475 (1994).
[12] B. Legras, P. Santangelo, and R. Benzi, "High-resolution numerical experiments for forced two-dimensional turbulence," Europhys. Lett. **5**, 37 (1988).
[13] H. Kellay, X. L. Wu, and W. I. Goldburg, "Experiments with turbulent soap films," Phys. Rev. Lett. **74**, 3975 (1995).
[14] T. Gotoh, "Energy spectrum in the inertial and dissipation ranges of two-dimensional steady turbulence," Phys. Rev. E **57**, 2984 (1998).
[15] E. Lindborg, T. M. Alvelius, and P. N. Guzdar, "The kinetic energy spectrum of the two-dimensional enstrophy turbulence cascade," Phys. Fluids **12**, 945 (2000).
[16] G. Boffetta, A. Celani, S. Musacchio, and M. Vergalossa, "Intermittency in two-dimensional Ekman-Navier-Stokes turbulence," Phys. Rev. E **66**, 026304 (2002).
[17] G. Boffetta, "Energy and enstrophy in the double cascade of two-dimensional turbulence," J. Fluid Mech. **589**, 253 (2007).
[18] C. H. Bruneau and H. Kellay, "Coexistence of two inertial ranges in two-dimensional turbulence," Phys. Rev. E **71**, 046305 (2005).
[19] C. H. Bruneau, P. Fischer, and H. Kellay, "The structures responsible for the inverse energy and the forward enstrophy cascades in two-dimensional turbulence," Europhys. Lett. **78**, 34002 (2007).
[20] C. H. Bruneau and P. Fischer, "Influence of the filtering tools on the analysis of two-dimensional turbulent flows," Comput. Fluids **38**, 1324 (2009).
[21] S. Chen, R. E. Ecke, G. L. Eyink, X. Wang, and Z. Xiao, "Physical mechanism of the two-dimensional enstrophy cascade," Phys. Rev. Lett. **91**, 214501 (2003).
[22] S. Chen, R. E. Ecke, G. L. Eyink, M. Rivera, M. Wan, and Z. Xiao, "Physical Mechanism of the two dimensional inverse energy cascade," Phys. Rev. Lett. **96**, 084502 (2006).
[23] P. Fischer, C. H. Bruneau, and H. Kellay, "Multiresolution analysis for 2D turbulence. Part 2: A physical interpretation," Discrete Contin. Dyn. Syst., Ser. B **4**, 717 (2007).
[24] M. Farge and G. Rabreau, "Transformee en ondelettes pour detecter et analyser les structures coherentes dans les ecoulements turbulents bidimensionnels," C. R. Acad. Sci. de Paris **307**, 1479 (1988).
[25] M. Farge and G. Rabreau, in *Scaling, Fractals and Nonlinear Variability in Geophysics*, edited by D. Schertzer (Meteorologie Nationale, Paris, 1988), pp. 11–16.
[26] J. Weiss, "The dynamics of enstrophy transfer in two-dimensional hydrodynamics," Physica D **48**, 273 (1991).
[27] H. Kellay and W. I. Goldburg, "Two-dimensional turbulence: a review of some recent experiments," Rep. Prog. Phys. **65**, 845 (2002).
[28] P. Angot, C. H. Bruneau, and P. Fabrie, "A penalization method to take into account obstacles in incompressible viscous flow," Numer. Math. **81**, 497 (1999).
[29] C. H. Bruneau and M. Saad, "The 2D lid-driven cavity problem revisited," Comput. Fluids **35**, 326 (2006).
[30] C. H. Bruneau and P. Fischer, "Spectra and filtering: A clarification," Int. J. Wavelets, Multiresolut. Inf. Process. **5**, 465 (2007).
[31] H. Clercx, "A spectral solver for the Navier-Stokes equations in the velocity-vorticity formulation for flows with two non-periodic directions," J. Comput. Phys. **137**, 186 (1997).
[32] H. Clercx and G. van Heijst, "Energy spectra for decaying 2D turbulence in a bounded domain," Phys. Rev. Lett. **85**, 306 (2000).
[33] H. Clercx, A. Nielsen, D. Torres, and E. Coutsias, "Two-dimensional turbulence in square and circular domains with no-slip walls," Eur. J. Mech. B/Fluids **20**, 557 (2001).
[34] G. Van Heijst, H. Clercx, and D. Molenaar, "The effects of solid boundaries on confined two-dimensional turbulence," J. Fluid Mech. **554**, 411 (2006).
[35] M. Wells, H. Clercx, and G. van Heijst, "Vortices in oscillating spin-up," J. Fluid Mech. **573**, 339 (2007).